

# Increasing the O<sub>2</sub> Resistance of the [FeFe]-Hydrogenase CbA5H through Enhanced Protein Flexibility

Andreas Rutz, Chandan K. Das, Andrea Fasano, Jan Jaenecke, Shanika Yadav, Ulf-Peter Apfel, Vera Engelbrecht, Vincent Fourmond, Christophe Léger, Lars V. Schäfer, and Thomas Happe\*



Cite This: *ACS Catal.* 2023, 13, 856–865



Read Online

ACCESS |



Metrics & More



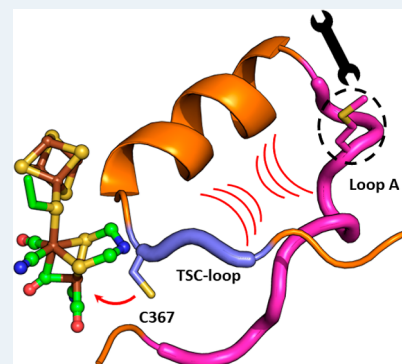
Article Recommendations



Supporting Information

**ABSTRACT:** The high turnover rates of [FeFe]-hydrogenases under mild conditions and at low overpotentials provide a natural blueprint for the design of hydrogen catalysts. However, the unique active site (H-cluster) degrades upon contact with oxygen. The [FeFe]-hydrogenase from *Clostridium beijerinckii* (CbA5H) is characterized by the flexibility of its protein structure, which allows a conserved cysteine to coordinate to the active site under oxidative conditions. Thereby, intrinsic cofactor degradation induced by dioxygen is minimized. However, the protection from O<sub>2</sub> is only partial, and the activity of the enzyme decreases upon each exposure to O<sub>2</sub>. By using site-directed mutagenesis in combination with electrochemistry, ATR-FTIR spectroscopy, and molecular dynamics simulations, we show that the kinetics of the conversion between the oxygen-protected inactive state (cysteine-bound) and the oxygen-sensitive active state can be accelerated by replacing a surface residue that is very distant from the active site. This sole exchange of methionine for a glutamate residue leads to an increased resistance of the hydrogenase to dioxygen. With our study, we aim to understand how local modifications of the protein structure can have a crucial impact on protein dynamics and how they can control the reactivity of inorganic active sites through outer sphere effects.

**KEYWORDS:** metalloenzymes, [FeFe]-hydrogenase, spectroscopy, protein film voltammetry, molecular dynamics



## INTRODUCTION

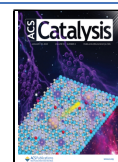
[FeFe]-hydrogenases catalyze the reversible oxidation and production of hydrogen at high rates.<sup>1,2</sup> These redox enzymes use a unique active center, the so-called “H-cluster”, which consists of two subclusters. The cubane subcluster, [4Fe]<sub>H</sub>, is a standard [4Fe–4S] cluster ligated by four cysteine ligands to the protein backbone. One of the cysteine ligands also bridges the [4Fe]<sub>H</sub> cluster and the binuclear FeS cluster, [2Fe]<sub>H</sub>, which is additionally coordinated by two CN<sup>−</sup> and three CO ligands.<sup>3,4</sup> Both iron atoms, Fe<sub>p</sub> and Fe<sub>d</sub> (the subscripts p and d refer to “proximal” and “distal” with respect to the cubane subcluster), are connected via an azadithiolate bridge (ADT), which plays an important role during the catalytic hydrogen turnover.<sup>3–6</sup> The vacant site at Fe<sub>d</sub> is involved in hydrogen oxidation/evolution and is prone to the binding of various inhibitors (O<sub>2</sub>, CO, and SH).<sup>7–14</sup> In contrast to industrial platinum-based hydrogen producing catalysts, [FeFe]-hydrogenases rely on earth-abundant metals such as iron and can be considered as biological blueprints for the design of synthetic catalysts.<sup>15–18</sup> However, their catalytic performance is limited by high O<sub>2</sub> sensitivity. The binding of oxygen to the vacant coordination site is coupled to further protonation and reduction steps that eventually lead to the formation of reactive oxygen species (ROS), which subsequently results in an irreversible destruction of the active site.<sup>7,8,19–22</sup> Note that in standard [FeFe]-hydrogenases, the

destruction of the enzyme by O<sub>2</sub> is mainly irreversible, but a partial reactivation, resulting from the reduction of O<sub>2</sub> at the active site, can be detected after a short exposure to O<sub>2</sub>.<sup>7,23</sup> Computational and experimental studies suggested that O<sub>2</sub> binding leads either to the decomposition of the [2Fe]<sub>H</sub> subsite, retaining an intact [4Fe]<sub>H</sub> site,<sup>21</sup> or to ROS (O<sub>2</sub><sup>−</sup>, OOH<sup>−</sup>) diffusion that initiates the decomposition at [4Fe]<sub>H</sub>.<sup>13,24</sup> However, a crystallographic study suggests that both pathways can coexist and are highly dependent on the electron supply.<sup>22</sup> The enzyme CbA5H from the bacterium *Clostridium beijerinckii* is so far the only characterized [FeFe]-hydrogenase, which tolerates a prolonged exposure to O<sub>2</sub>, by reversibly switching between the active H<sub>ox</sub> state to the inactive but O<sub>2</sub>-protected H<sub>inact</sub> state.<sup>25,26</sup> The H<sub>inact</sub> state was originally identified in DdH from *Desulfovibrio desulfuricans* and provided an irreversible protection against O<sub>2</sub>, albeit only limited to the first reductive reactivation.<sup>27,28</sup> Studies by Rodríguez-Maciá et al. could provide evidence that this effect is attributed to the binding of exogenous sulfide under oxidizing conditions.<sup>9</sup>

**Received:** August 15, 2022

**Revised:** December 8, 2022

**Published:** December 28, 2022



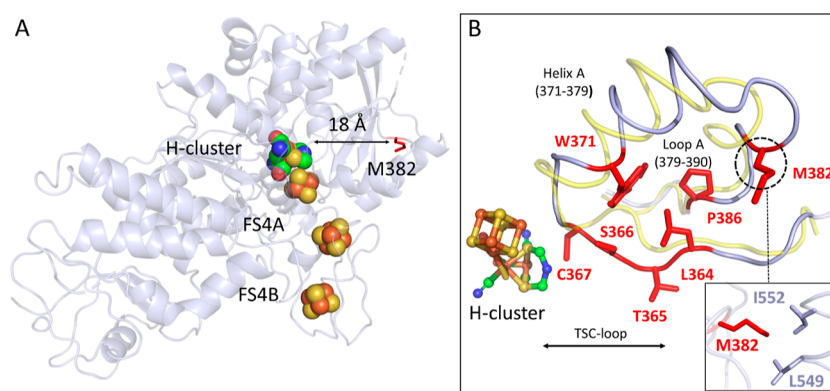


**Figure 1.** Structural overview of the [FeFe]-hydrogenase CbASH<sup>WT</sup>. (A) X-ray structure of CbASH<sup>air</sup> (PDB: 6TTL) shown as a cartoon. H-cluster and accessory FeS clusters are depicted as spheres. Residue M382 is represented as a stick in red. (B) Structural alignment of CpI (PDB: 4XDC, yellow) and CbASH<sup>air</sup> (light blue). H-cluster and residues that are expected to influence the loop flexibility are depicted as sticks and highlighted in red. Inset shows residues that are in close vicinity to M382 as sticks.

Sulfide treatment to other [FeFe]-hydrogenases could reproduce this inactivation, enabling an effective protection against O<sub>2</sub> prior to the first reactivation.<sup>10,29</sup> In contrast to this, CbASH possesses an intrinsic protection mechanism toward O<sub>2</sub>, independent of exogenous sulfide, which is governed by the coordination of an adjacent cysteine residue (C367). Upon oxidizing conditions, C367 can coordinate to Fe<sub>d</sub> and thus prevent the binding of O<sub>2</sub> and the subsequent destruction of the active site.<sup>25,26,30</sup> It has been shown that various residues are crucial for the movement of the cysteine residue and, based on spectroscopic and kinetic data, we proposed a detailed model for the conformational change of the “TSC” peptide loop that relocates the conserved cysteine close enough to Fe<sub>d</sub> to allow coordination.<sup>30</sup>

A structural comparison of CbASH and the standard [FeFe]-hydrogenase CpI from *Clostridium pasteurianum* unveiled a complex interplay of different residues which prevent the coordination of the cysteine residue in conventional [FeFe]-hydrogenases. Substituting these amino acids with the analogues of CpI resulted in slower conformational changes and more O<sub>2</sub>-sensitive CbASH variants. In the WT enzyme, the reductive reactivation is limited to a few cycles of O<sub>2</sub> exposure and reductive reactivation: a fraction of the enzyme is irreversibly degraded in each reversible conversion from active (A) to inactive (I) form, as observed in independent investigations of CbASH.<sup>26</sup> In this work, we show that methionine 382, an amino acid positioned more than 18 Å away from the active site (see Figure 1A), is an important structural determinant of O<sub>2</sub> resistance in CbASH. Due to the inherent properties of methionine residues, M382 anchors the protein framework and stabilizes a particular configuration of the peptide chain. A substitution of this residue results in structural changes within the protein, which increase the flexibility of the loop (termed “Loop A”) adjacent to the TSC loop. By combining site-directed mutagenesis, IR spectroscopy, molecular dynamics simulations, and electrochemical kinetic studies, we show that the residue at position 382 remotely controls the active site chemistry of CbASH and that its substitution to glutamic acid accelerates the conformational changes and renders the enzyme more resistant to oxygen.

## EXPERIMENTAL SECTION

**Site-Directed Mutagenesis.** QuikChange PCR was used to generate hydrogenase genes with different codons according to the protocol described earlier.<sup>31</sup> Expression plasmids were amplified by using mismatch primers (Table S1). The products were treated with endonucleases DpnI and transformed into *Escherichia coli* strain DH5 $\alpha$  by using the heat shock method. All DNA constructs were subsequently verified by sequencing.

**Expression and Purification.** The *E. coli* strain BL21 (DE3)  $\Delta$ iscR was transformed with the expression plasmid pET21b containing the codon-optimized CBASH gene (NCBI GenBank: KX147468.1) and was used to express apo CbASH (lacking the [2Fe<sub>H</sub>] subcluster).<sup>32</sup> Expression and purification were conducted under strictly anaerobic conditions as described previously.<sup>33</sup> Affinity chromatography was performed using Strep-Tactin high-capacity resin (IBA GmbH). The protein concentration was determined by Bradford assay,<sup>34</sup> and purity was verified by SDS-PAGE (polyacrylamide gel electrophoresis).<sup>35</sup> Proteins were stored at  $-80$  °C in 100 mM Tris-HCl buffer pH 8 with 2 mM sodium dithionite (NaDT).

**In Vitro Maturation.** Apoproteins were incubated on ice for 1 h with a 10-fold molar excess of the artificially synthesized [2Fe]<sub>H</sub> cofactor mimic ([2Fe<sub>2</sub>[ $\mu$ -(SCH<sub>2</sub>)<sub>2</sub>NH]-(CN)<sub>2</sub>(CO)<sub>4</sub>]<sup>2-</sup>)<sup>36</sup> in order to reconstitute the active protein, as described earlier.<sup>37</sup> Holoproteins and excess [2Fe]<sub>H</sub> were separated by size exclusion chromatography (NAP 5 column, GE healthcare).

**Enzyme Activity Assay (H<sub>2</sub> Production) with Multiple Inactivation Cycles.** H<sub>2</sub> production activity was assayed with 10 mM methyl viologen (MV) as the electron mediator, 200 mM NaDT as the electron donor, and 400 ng holoenzyme in 100 mM potassium phosphate buffer (K<sub>2</sub>HPO<sub>4</sub>/KH<sub>2</sub>PO<sub>4</sub>) at pH 6.8. The reaction mixture was degassed with 100% argon and incubated for 20 min at 37 °C in a sealed 8 mL glass vessel. The amount of H<sub>2</sub> was determined by gas chromatography. The inactivation was performed by incubating the enzyme solution for 15 min under an atmosphere of air, on ice, making sure the solution is aerated. After the first inactivation and prior to every further inactivation with air, the solution was treated for 20 min with 100% H<sub>2</sub> in order to ensure full activation. All protein solutions were prepared in the absence of NaDT. After each inactivation, aliquots were taken for subsequent standard in vitro assays, as described

before. Each measurement was performed in triple determination with three technical replicates.

**Protein Film Electrochemistry.** Cyclic voltammetry and the amperometry experiments employed to elucidate the kinetics of the conformational change leading to  $H_{\text{inact}}$  formation were carried out in a JACOMEX glovebox filled with  $N_2$  in a thermostated ( $T = 5\text{ }^\circ\text{C}$ ) electrochemical cell with two compartments. The main compartment contained the rotating working electrode (pyrolytic graphite edge, 3 mm diameter, typical rotation rate, 3000 rpm, mounted on a Pine MSR rotator) and the counter electrode (a platinum wire) as well as the inlet of  $H_2$ . The main compartment was filled with a mixed buffered solution (consisting of 5 mM of each MES, HEPES, sodium acetate, TAPS, and CHES and 0.1 M NaCl). The main compartment was connected via a Luggin capillary to a second compartment, containing the calomel reference electrode in 0.1 M NaCl. All potentials are quoted with respect to the standard hydrogen electrode, calculated using  $E_{\text{SHE}} = E_{\text{calomel}} + 0.241\text{ V}$ . To prepare the protein films, the pyrolytic graphite “edge” (PGE) rotating disk working electrode was polished with an aqueous alumina slurry (Buehler, 1  $\mu\text{m}$ ), rinsed, painted with 0.5  $\mu\text{L}$  of an enzyme solution ( $\sim 5\text{ mg/mL}$  in 100 mM Tris–HCl, pH 8, with 2 mM NaDT), and let to dry for 2 min. The measured catalytic currents were between 1 and 10  $\mu\text{A}$ , so that the mass transport toward the rotating electrode was not limiting.<sup>38</sup> Cyclic voltammetry (CV) and chronoamperometric experiments were recorded with the program GPES and analyzed with the open-source program QSoas.<sup>39</sup> Chronoamperometric experiments were started and ended at a potential 30 mV below the  $H^+/H_2$  equilibrium potential (pH 7:  $-0.459\text{ V}$  vs SHE) to ensure the complete activation of the enzyme film. The intermediate steps at the oxidative potential were of 100 mV amplitude. Before analyzing the changes in  $H_2$  oxidation current, we subtracted the background capacitive current recorded in a control experiment without the enzyme.

**ATR–FTIR Spectroscopy.** Attenuated total reflectance Fourier transform infrared (ATR–FTIR) spectroscopy was performed, using a Bruker Tensor II spectrometer (Bruker Optik, Germany) equipped with a 9 reflection ZnSe/Si crystal (Microm ATR Vision, Czitek). All measurements were conducted under anoxic conditions (1.5%  $H_2$ , 98.5%  $N_2$ ) at 25  $^\circ\text{C}$ . The FTIR spectra were recorded from 4000 to 1000  $\text{cm}^{-1}$  with a resolution of 2  $\text{cm}^{-1}$ . The protein film was dried with a  $H_2$  gas stream for around 10 min and re-humidified with an aerosol by purging a buffer-containing compartment.

**Molecular Dynamics Simulations.** All molecular dynamics (MD) simulations were performed with GROMACS version 2021.4.<sup>40</sup> The structure of the H domain was taken from the previously reported crystal structure of WT CbASH captured in the  $H_{\text{inact}}$  state (PDB ID 6TTL).<sup>30</sup> The M382E variant structure was generated by replacing the M382 side chain in 6TTL. The CHARMM36 force field was employed for the protein together with the CHARMM-specific TIP3P water model. The force field parameters for the H cluster and other Fe–S clusters were taken from the work of Chang et al. and McCullagh et al.<sup>41,42</sup> The  $H_{\text{ox}}$  state was simulated, with the C367 side chain protonated ( $-\text{SH}$ ). The protein structures were solvated in dodecahedron-shaped periodic simulation boxes filled with 13,206 water molecules and sodium ions to neutralize the systems. Prior to the MD simulations, the systems were energy-minimized, followed by stepwise equilibration for 2.7 ns, during which harmonic position restraints

were applied to different sets of atoms. In the first  $NVT$  equilibration phase (0.2 ns), position restraints with force constants of 1000  $\text{kJ/mol/nm}^2$  were applied to all non-hydrogen atoms of the protein and the Fe–S clusters. Subsequently, the second equilibration phase was continued for another 2.5 ns in the  $NpT$  ensemble. During the initial 0.5 ns of this second equilibration phase, the position restraints were still applied to all nonhydrogen atoms of the protein and the Fe–S clusters. During the final 2.0 ns, the position restraints were only applied to all nonhydrogen atoms of the protein backbone. The MD simulations were conducted within the periodic boundary conditions in the  $NpT$  ensemble at a constant temperature of 300 K and 1 bar pressure, by coupling to the velocity-rescaling thermostat of Bussi and co-workers and a weak coupling barostat, respectively.<sup>43,44</sup> The Coulomb and Lennard-Jones interactions were described with a buffered Verlet pair list with a 1.2 nm cutoff, with the forces smoothly switched to zero between 1.0 and 1.2 nm.<sup>45</sup> Long-range electrostatic interactions were treated with the particle mesh Ewald method with 0.12 nm grid spacing.<sup>46</sup> The LINCS and SETTLE constraint algorithms were employed to constrain all protein bonds involving H atoms and internal degrees of freedom of water molecules, respectively, allowing to integrate the equations of motion with 2 fs time steps.<sup>47,48</sup> Finally, starting with the equilibrated systems, two 1500 ns production MD simulations for each of the two different systems (WT enzyme, M382E) were carried out in the  $NpT$  ensemble, initiated with different random seeds to generate the initial atomic velocities from the Maxwell distribution at 300 K. Because the starting structures of the  $H_{\text{ox}}$  states were built from the  $H_{\text{inact}}$  crystal structure, the initial 200 ns of each simulation was considered to be equilibration and discarded in the analyses.

## RESULTS AND DISCUSSION

We focus on the position of methionine 382, which is located in a bridging position between Helix A and Loop A, close to the TSC loop (Figure 1B). The crystal structure of CbASH suggests that M382 forms hydrophobic contacts with residues L549 and I552 (Figure 1B, inset), which might coordinate the peptide chain. Methionine residues often stabilize protein structures by forming hydrophobic interactions with the nearby residues.<sup>49,50</sup> The highly flexible side chain with the unique properties of the thioether sulfur render this amino acid as highly versatile.<sup>49,51–53</sup> It was proposed that methionines form tighter van der Waals contacts than other hydrophobic side chains, which provide a natural anchor point in the protein environment.<sup>54</sup> The replacement of a methionine can abolish such interactions and therefore may increase the flexibility of peptide chains.<sup>49</sup> We aimed to alter the protein structure at this position by replacing M382 and studying the influence of the mutation on the conformational dynamics and on the (in)activation mechanism.

**Enhanced  $O_2$  Stability of the M382E Variant.** We replaced M382 with glutamic acid, isoleucine, and alanine. The M382A variant did not exhibit a measurable activity, while the isoleucine exchange maintained a high catalytic performance. The exchange of methionine to glutamic acid (M382E) resulted in an  $H_2$  production activity of about 50–60% compared to the CbASH<sup>WT</sup> protein. We investigated the stability of the variant M382E after repeated cycles of exposure to air and  $H_2$  using MV-based  $H_2$  production assays.

The results in Figure 2 show a decrease in activity after each exposure to air for the WT and the variant. The observed

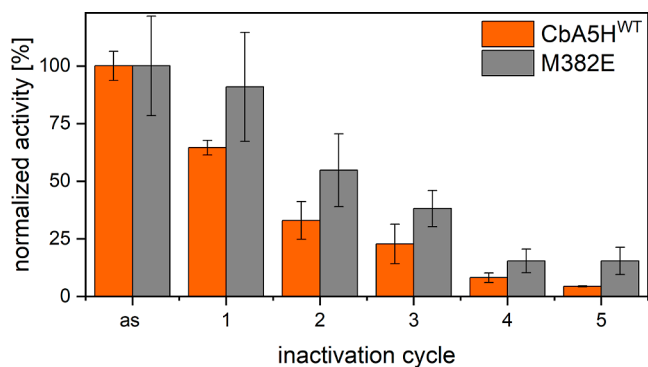


**Figure 2.** H<sub>2</sub> production activities after aerobic inactivation of CbA5H<sup>WT</sup> and M382E. Normalized activity of three independent measurements after cycles of air exposure (15 min at 4 °C). After every inactivation step, the protein solution was reactivated under 100% H<sub>2</sub> atmosphere for 20 min. Individual data sets are summarized in Figure S3 and Table S2.

decay of CbA5H<sup>WT</sup> activity is in agreement with earlier reports (~40% after the first exposure and ~75% after the second exposure<sup>26</sup>). However, the relative decrease in activity is smaller for the M382E variant and indicates an improved protection, which might be associated with the easier or faster coordination of the C367 side chain to the distal Fe.

**Influence of M382E Substitution on the Catalytic Cycle.** We examined the protein variants using FTIR spectroscopy to assess the extent of incorporation of the [2Fe]<sub>H</sub> subsite into the protein and to monitor the catalytically relevant redox states. We observed a reduced H-cluster occupancy in the M382E variant which is consistent with the reduced activity (see Figure S4). The difference spectrum in Figure 3A shows that the treatment of the WT enzyme with a hydrogen-saturated aerosol led to the accumulation of the bands at 1893, 1916, 2040, and 2075 cm<sup>-1</sup>, which are assigned to the H<sub>red</sub>H<sup>+</sup> state with minor contributions of H<sub>hyd</sub> and H<sub>ox</sub>.

The H<sub>red</sub>H<sup>+</sup> state features a reduced [2Fe]<sub>H</sub> and a proton bound to the ADT bridge.<sup>55,56</sup> A one-electron reduction leads

to the formation of the H<sub>red</sub>H<sup>+</sup> state, which enables the subsequent formation of the H<sub>hyd</sub> state, featuring a terminal hydride species bound to Fe<sub>d</sub>.<sup>57</sup> In contrast to that, we could observe that the spectrum of the M382E variant exhibited a significant contribution of the H<sub>hyd</sub> state (2091, 2083, 1979, 1963, and 1855 cm<sup>-1</sup>) after a prolonged exposure to hydrogen (Figure 3).

Standard [FeFe]-hydrogenases accumulate this intermediate usually in proton transfer-deficient variants or under acidic conditions in combination with an atmosphere of H<sub>2</sub>.<sup>57</sup> The accumulation of H<sub>hyd</sub> in the M382E variant might suggest a conformational change of the native proton transfer pathway (PTP). This notion is supported by our MD simulations (see below), which show that in the M382E variant, residue S387, which is a key residue in the native PTP, is dislocated and no longer participates in an H-bond network with E341 and E344, which would be required for an efficient proton transfer along this pathway (Figure S5). We speculate that the enhanced spatial freedom influences the protonation dynamics of the H cluster, hence providing a reasonable explanation for the H<sub>hyd</sub> accumulation in M382E. Previous studies could report a similar observation for proton transfer-deficient CpI variants, which exhibited an increased population of the hydride-bound state.<sup>57,58</sup> Additionally, it could be shown that an impaired protonation of O<sub>2</sub><sup>-</sup> species due to an interrupted PTP prevents the formation of mobile ROS and reduces the degradation of the H cluster.<sup>19</sup> The structural deviations in the PTP of the variant M382E and the resulting presence of a terminal-bound hydride might support the resistance toward oxygen. The subsequent exposure of the enzymes to air led to the formation of the O<sub>2</sub>-protected H<sub>inact</sub> state (2107, 2080, 2011, 1991, and 1840 cm<sup>-1</sup>).

**M382E Substitution Changes the Conformational Dynamics of the Protein.** To understand how the mutation at site 382 modulates the conformational ensembles of CbA5H, we carried out all-atom MD simulations of the WT enzyme and the M382E variant. The simulations were started from the H<sub>ox</sub> state, which corresponds to the A<sub>1</sub> state (see below). The MD simulations were based on the X-ray crystal structure of CbA5H from *C. beijerinckii* (PDB code 6TTL). The atomic coordinates of the M382E variant were generated from the crystal structure by replacing the M382 side chain. Figure 4A–C shows that in the M382E variant, Loop A undergoes structural changes, which also affect the vicinity of the TSC loop. This conformational change is triggered by solvation forces, which displace the charged E382 side chain from the hydrophobic environment in which M382 is located in the WT protein, such that E382 becomes fully hydrated by moving away from the helix bearing the hydrophobic contact-forming residue L549 (Figure 4B–D). This conformational change goes along with a pronounced increase of the structural flexibility in this region (see RMSF profile showing the fluctuations of the residues in Figure 4E). Besides residue S387 of the PTP, this part of the peptide chain bears a residue that is relevant for the positioning of C367 near Fe<sub>d</sub> (P386) and may influence the kinetics of cysteine coordination to Fe<sub>d</sub>. These observations are in line with our previous results, which suggested that at least three distinct positions (L364, P386, and A561) are crucial for the conformational change.<sup>30</sup> To further investigate the link between the structural dynamics and the inactivation kinetics, we employed protein film electrochemistry (PFE).

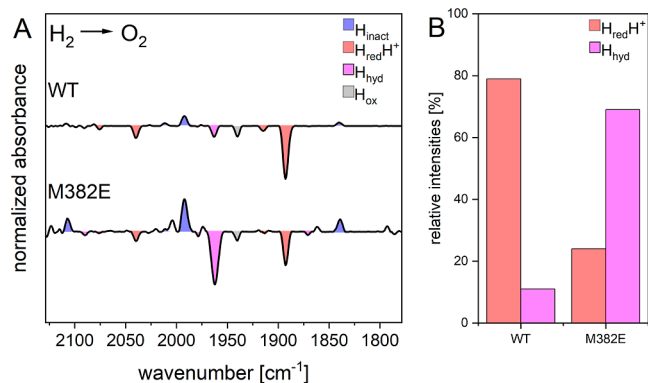


**Figure 3.** IR frequencies of CbA5H<sup>WT</sup> and M382E. (A) ATR-FTIR difference spectra of CbA5H<sup>WT</sup> and M382E (200–500 μM, 0.1 M potassium phosphate buffer, pH 7) after 100% H<sub>2</sub> gassing and after treatment with air. Blue (H<sub>inact</sub>), red (H<sub>red</sub>H<sup>+</sup>), purple (H<sub>hyd</sub>), and gray (H<sub>ox</sub>). (B) Relative band intensities of WT protein and variant with respect to the relative absorbance spectra.

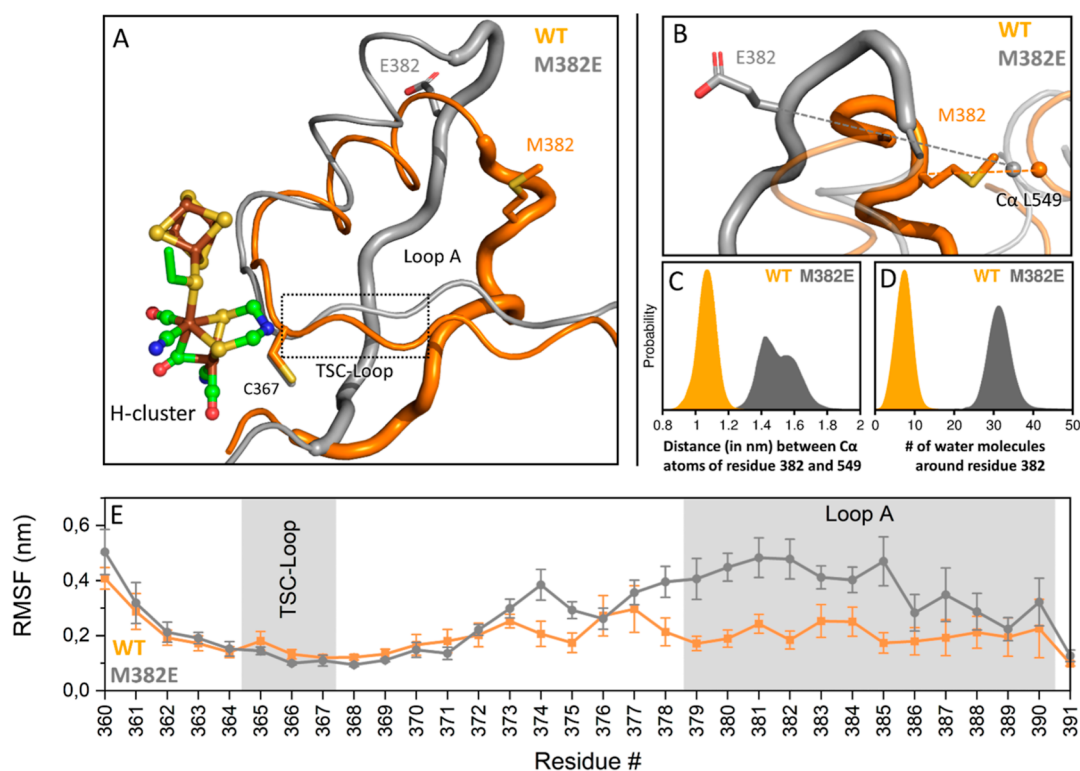


**Figure 4.** MD simulations of CbASH<sup>WT</sup> and M382E. (A) Cartoon representation of CbASH showing the WT protein in orange and M382E variant in gray. H-cluster and residues C367, M382 (CbASH<sup>WT</sup>), and E382 (M382E variant) are shown as sticks. Loop A is shown in thick, and the TSC loop is indicated by a box. (B) Structural overlay of representative snapshots from the MD simulations of WT and the M382E variant. Distances between C $\alpha$  atoms of residues 382 and 549 are indicated by dashed lines. (C) Histogram of the distance between C $\alpha$  atoms of residues 382 and 549 in CbASH<sup>WT</sup> and M382E variant. (D) Number of water molecules around residue 382 in CbASH<sup>WT</sup> and variant. A water molecule was counted if its O atom was within 0.5 nm of any atom of residue 382. (E) RMSF plot depicting the fluctuations of the residues in WT and M382E. The TSC loop and Loop A are highlighted with gray boxes.

### Position M382 Influences Anaerobic Inactivation.

PFE was used to examine the kinetics of the conformational changes that lead to reversible inactivation in CbASH<sup>WT</sup> and the variant, using the method described earlier.<sup>30</sup> The activity of the enzyme adsorbed onto a graphite electrode is measured as a current following sweeps or steps of the applied potential, which trigger its (in)activation. All electrochemical experiments were performed at 5 °C to minimize film loss. Figure 5 compares the cyclic voltammograms of the WT protein and the M382E variant (see Figure S7 for the M382I variant and Figure S8 for the effect of varying the scan rate).

In both cases, a negative current reveals H<sub>2</sub> production at a low potential, and H<sub>2</sub> oxidation is seen as a positive current at a high potential. The current response is dependent on the direction of the sweep (the CV plots show a very pronounced hysteresis). The H<sub>2</sub> oxidation current decreases at a low potential (positive of the H<sup>+</sup>/H<sub>2</sub> Nernst potential) due to oxidative inactivation, and the enzymes reactivate during the reductive sweep. These processes are slow on the voltammetric timescale, hence the hysteresis. The high potential inactivation observed with CbASH differs from that observed with standard hydrogenases: it occurs at a much lower potential than that of standard hydrogenases, and it is not due to the presence of chloride anions in the buffer (Figure S9 in ref 30 for the WT and Figure S9 for the M382E mutant).

The inactivation of CbASH<sup>WT</sup> disappears when C367 is replaced with aspartate and was therefore related to the formation of the H<sub>inact</sub> state.<sup>30</sup> Figure 5 shows that the (in)activation of the variant is more pronounced. The kinetics

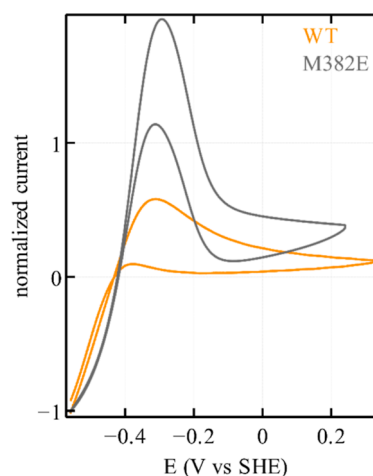


**Figure 5.** Cyclic voltammograms showing the anaerobic (in)activation of CbASH (orange) and the M382E variant (gray) under conditions of direct electron transfer with a rotating disk pyrolytic graphite edge electrode (pH 7, 5 °C, 1 bar H<sub>2</sub>, scan rate 20 mV/s, electrode rotation rate 3000 rpm). See Figure S7 for the comparison between the data obtained with CbASH and the M382I variant. Note that in protein film voltammetry, the magnitude of the signal cannot be interpreted because it depends on the unknown enzyme coverage. Only the shape of the signal matters, and therefore the potential chosen for the normalization of the current is arbitrary. See Figure S6 A for the raw (non-normalized) data plotted in this figure.

of the transformation is easily assessed by interpreting the potential step experiments such as those in Figure 6B, where

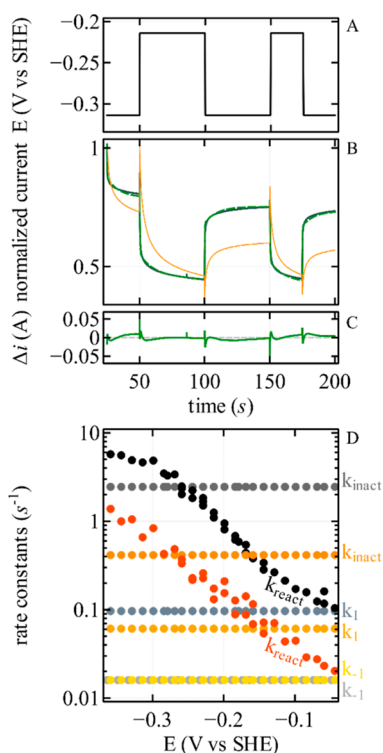


**Figure 6.** Potential step experiments used to quantify the anaerobic inactivation kinetics of CbASH<sup>WT</sup> and the M382E variant. See Figures S11 and S12 for the comparison between the data obtained with CbASH and the M382I variant. (A) Example of potential steps applied to the electrode onto which the enzymes are adsorbed (pH 7, 5 °C, 1 bar H<sub>2</sub>, 3000 rpm). (B) Current responses (orange: WT, gray: M382E) to the potential steps in panel (A). The best fit of the model is described earlier and is shown in dashed green.<sup>30</sup> (C) Residual of the fit. (D) Four rate constants determined by fitting the model to a series of chronoamperograms obtained with different potential steps (see Figure S10). Three rate constants are potential-independent and shown with dark orange, orange, and yellow circles ( $k_{\text{inact}}$ ,  $k_1$ , and  $k_{-1}$ , respectively) for the WT protein and in gray, slate gray, and dark gray ( $k_{\text{inact}}$ ,  $k_1$ , and  $k_{-1}$ , respectively) for the M382E mutant.  $k_{-1}$  is ill-defined (cannot be accurately determined) and was set to the same value for both enzymes. The values of  $k_{\text{react}}$  are shown as red and black circles for the WT enzyme and for the mutant, respectively. The WT data are replotted from ref 30.

the electrode potential is repeatedly stepped up and down, and the current response is analyzed using a kinetic model. Note in

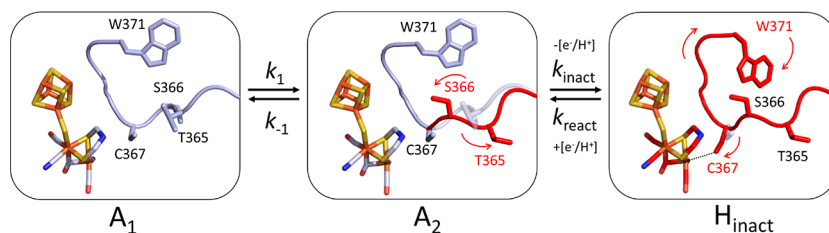


**Figure 7.** AAI model for the reversible conversion between active and inactive forms of CbASH<sup>WT</sup>. Structural alignment of CpI (A<sub>1</sub>, light blue) and CbASH<sub>air</sub> (H<sub>inact</sub>; red). Three main states are identified:<sup>30</sup> the active species A<sub>1</sub>, a second active species A<sub>2</sub> after the conformational change of the TSC loop (central panel), and the inactive species H<sub>inact</sub> where C367 is coordinated to Fe<sub>d</sub>. Arrows indicate the rate constants  $k_1$ ,  $k_{-1}$ ,  $k_{\text{inact}}$ , and  $k_{\text{react}}$ .

this figure that the change in current following the potential steps is faster for the variant than the WT.

The previously established kinetic model<sup>30</sup> considers three distinct species (A<sub>1</sub>, A<sub>2</sub>, and I; Figure 7) and accounts for the biphasic kinetic traces that are observed in chronoamperometry experiments. “A<sub>1</sub>” and “A<sub>2</sub>” are the active forms of the enzyme; “I” is an inactive form, the “H<sub>inact</sub> state”, in which cysteine C367 is coordinated to the distal iron, competing with hydrogen binding and thus preventing turnover. The potential-independent rate constants  $k_1$  and  $k_{-1}$  describe the conversion between A<sub>1</sub> and A<sub>2</sub>. Due to the slow transition between these two forms ( $1/(k_1 + k_{-1}) \approx 10$  s), we proposed that this step is associated with a conformational change. The final coordination of the cysteine ligand itself occurs during the transformation of A<sub>2</sub> to I, and the bond is labile ( $1/(k_{\text{inact}} + k_{\text{react}}) \approx 1$  s) due to the relatively long distance of 3.1 Å. Note that the inactive state is formed upon anaerobic or aerobic oxidation and provides effective protection against O<sub>2</sub>. Hence, the faster the inactivation, the more resistant the enzyme is. This correlation has already been observed in our previous work, although the mutants examined therein were slower to inactivation and thus less O<sub>2</sub>-resistant.<sup>30</sup> The second step involves the transfer of one proton and one electron, but the analysis of the data shows that only the backward rate constant  $k_{\text{react}}$  is potential-dependent (see ref 30 and Figure 6). We analyzed a number of chronoamperometric traces such as those in Figure 6B (see Figure S10) to measure the rate constants of interconversion between the active and inactive forms of the enzymes under various conditions of electrode potential. The results are shown in Figure 6D for the WT protein and the M382E variant (see S12 for the M382I variant). The results in Table 1 show that the M382E mutation

**Table 1.** Values of  $k_1$ ,  $k_{-1}$ ,  $k_{\text{react}}$ , and  $k_{\text{inact}}$  for CbASH<sup>WT</sup> and M382E<sup>a</sup>

	$k_1$ (s <sup>-1</sup> )	$k_{-1}$ (s <sup>-1</sup> )	$k_{\text{inact}}$ (s <sup>-1</sup> )	$k_{\text{react}}$ (s <sup>-1</sup> )	$k_{\text{inact}}/k_{\text{react}}$
CbASH <sup>WT</sup>	0.061	0.016	0.42	0.17	2.5
M382E	0.096	0.016	2.45	0.81	3.0

<sup>a</sup>Measured at pH7, 5 °C. All rate constants are potential-independent, except  $k_{\text{react}}$  which is given here at  $E = -199$  mV vs SHE. The value of  $k_{-1}$  is the least well-defined in the fitting procedure (as observed previously<sup>30</sup>) and was fixed to the WT. The WT data are taken from ref 30.

has no significant effect on the  $k_1/k_{-1}$  transition (note that, as mentioned in our previous work,  $k_{-1}$  cannot be accurately determined and was fixed to the WT protein value in all fitting procedures), but it increases the rate constants  $k_{\text{inact}}$  and  $k_{\text{react}}$

about 5.5-fold, respectively, leaving the ratio unchanged. The 5.5-fold acceleration corresponds to a 4 kJ/mol decrease in activation energy of step 2. Together with the increased structural flexibility observed in the MD simulations (see above), this provides a reasonable explanation why C367 coordinates faster to Fe<sub>4</sub> in the M382E variant than in the WT. The dynamic conversion between the different states (A<sub>1/2</sub> ↔ H<sub>inact</sub>) determines the efficiency of the inactivation mechanism of CbASH. Our study illustrates how the replacement of a residue is associated with an increased local flexibility of Loop A, which directly affects the TSC loop and thus the catalytic properties of the enzyme.

It is reported that local perturbations can affect protein dynamics over large distances (>25 Å),<sup>59</sup> with implications on different biological processes.<sup>60,61</sup> Loops, which are structurally relevant elements for protein stability,<sup>62,63</sup> specificity,<sup>64</sup> and protein–protein interactions,<sup>65</sup> often facilitate allosteric communication<sup>66</sup> and catalysis.<sup>67</sup> Detailed studies of various enzymes provide important insights into the role of protein dynamics in catalysis. In enzymes such as protein tyrosine phosphatase, a wide range of conformational changes can be observed, and loop flexibility can be significantly affected by the sequence composition.<sup>66,68,69</sup> Similar loop dynamics were studied in *Escherichia coli* dihydrofolate reductase EcDHFR, showing that two dynamically coupled loops play a critical role in controlling protein dynamics and function.<sup>59</sup> Experimental and computational works suggested a dynamic network that includes residues that remotely control catalysis and dynamic fluctuations of the loops.<sup>59,70</sup> On the other hand, allosteric effects are rarely reported for metalloproteins. For the FeS protein family mitoNEET, conformational changes of a loop 20 Å away from the metal center showed to affect the properties of the metal center.<sup>71</sup> Our observations in the [FeFe]-hydrogenase CbASH complement several previous studies, showing that the coupled networks of amino acids exist in proteins and that distant effects can influence active site events.

## CONCLUSIONS

Until now, two independent H<sub>inact</sub>-forming protection mechanisms are known in [FeFe]-hydrogenases, both of which rely on the protective function of the thiol groups that are coordinated to the vacant site of the H cluster. While the initially described sulfide-dependent inactivation is enabled due to the presence of sulfide in sulfate-reducing microorganisms like *D. desulfuricans*, CbASH developed an intriguing inactivation mechanism on the basis of a flexible cysteine side chain that can coordinate to the H-cluster. Both examples represent a convergent mechanism to resist O<sub>2</sub> and may result as a consequence of their ecological niche. This work demonstrates how individual amino acid exchanges can influence the catalytic properties of enzymes, even though they are located far away from the active site. Using site-directed mutagenesis, we investigate how local changes in the protein network can alter the dynamic interplay of the protein environment and fine-tune the intrinsic O<sub>2</sub> tolerance of CbASH. Our results contribute to the understanding of long-range effects and their modulation of dynamical conformational changes with respect to the prominent O<sub>2</sub> protection mechanism of CbASH. With these findings, we aim to provide new mechanistic insights into the development of advanced hydrogen catalysts for biotechnological purposes.

## ASSOCIATED CONTENT

### Supporting Information

The Supporting Information is available free of charge at <https://pubs.acs.org/doi/10.1021/acscatal.2c04031>.

FTIR spectra, in solution assays, and detailed kinetic characterization of the protein variants with PFE (PDF)

## AUTHOR INFORMATION

### Corresponding Author

Thomas Happe – Photobiotechnology, Department of Plant Biochemistry, Ruhr-Universität Bochum, 44801 Bochum, Germany; [orcid.org/0000-0003-1206-5234](https://orcid.org/0000-0003-1206-5234); Email: [thomas.happe@rub.de](mailto:thomas.happe@rub.de)

### Authors

Andreas Rutz – Photobiotechnology, Department of Plant Biochemistry, Ruhr-Universität Bochum, 44801 Bochum, Germany

Chandan K. Das – Theoretical Chemistry, Ruhr-Universität Bochum, 44801 Bochum, Germany; [orcid.org/0000-0003-3498-0425](https://orcid.org/0000-0003-3498-0425)

Andrea Fasano – Laboratoire de Bioénergétique et Ingénierie des Protéines, CNRS, Aix-Marseille Université, Institut de Microbiologie de la Méditerranée, 13009 Marseille, France; [orcid.org/0000-0002-8322-1620](https://orcid.org/0000-0002-8322-1620)

Jan Jaenecke – Photobiotechnology, Department of Plant Biochemistry, Ruhr-Universität Bochum, 44801 Bochum, Germany; Present Address: Technical University of Munich Campus Straubing for Biotechnology and Sustainability, Professorship for Electrobiotechnology, Uferstrasse 53, 94315 Straubing, Germany

Shanika Yadav – Inorganic Chemistry I, Department of Chemistry and Biochemistry, Ruhr-Universität Bochum, 44801 Bochum, Germany

Ulf-Peter Apfel – Inorganic Chemistry I, Department of Chemistry and Biochemistry, Ruhr-Universität Bochum, 44801 Bochum, Germany; Fraunhofer UMSICHT, 46047 Oberhausen, Germany; [orcid.org/0000-0002-1577-2420](https://orcid.org/0000-0002-1577-2420)

Vera Engelbrecht – Photobiotechnology, Department of Plant Biochemistry, Ruhr-Universität Bochum, 44801 Bochum, Germany

Vincent Fourmond – Laboratoire de Bioénergétique et Ingénierie des Protéines, CNRS, Aix-Marseille Université, Institut de Microbiologie de la Méditerranée, 13009 Marseille, France; [orcid.org/0000-0001-9837-6214](https://orcid.org/0000-0001-9837-6214)

Christophe Léger – Laboratoire de Bioénergétique et Ingénierie des Protéines, CNRS, Aix-Marseille Université, Institut de Microbiologie de la Méditerranée, 13009 Marseille, France; [orcid.org/0000-0002-8871-6059](https://orcid.org/0000-0002-8871-6059)

Lars V. Schäfer – Theoretical Chemistry, Ruhr-Universität Bochum, 44801 Bochum, Germany; [orcid.org/0000-0002-8498-3061](https://orcid.org/0000-0002-8498-3061)

Complete contact information is available at: <https://pubs.acs.org/doi/10.1021/acscatal.2c04031>

### Notes

The authors declare no competing financial interest.

## ACKNOWLEDGMENTS

This project received funding from the European Union's Horizon 2020 research and innovation program under the Marie Skłodowska-Curie grant agreement no. 801459—FP-

RESOMUS and was funded by the Deutsche Forschungsgemeinschaft (DFG) under Germany's Excellence Strategy—EXC 2033—390677874—RESOLV, the CNRS, and Aix Marseille University. T.H. thanks Volkswagen Stiftung (Az 98621) and the DFG for funding (HA 2555/10-1 & AP242/12-1). The authors thank Studienstiftung des deutschen Volkes for supporting A.R. S.Y. thanks DAAD for funding. The authors thank Christina Felbek for her help with the electrochemical measurements.

## ABBREVIATIONS

ADT, azadithiolate; FeS, iron–sulfur; ATR–FTIR, attenuated total reflectance Fourier transform infrared; IR, infrared; NaDT, sodium dithionite; MV, methyl viologen; CV, cyclic voltammetry;  $[2\text{Fe}]_{\text{H}}$ ,  $([2\text{Fe}_2[\mu-(\text{SCH}_2)_2\text{NH}]-(\text{CN})_2(\text{CO})_4]^{2-})$ ; PFE, protein film electrochemistry

## REFERENCES

- (1) Hexter, S. V.; Grey, F.; Happe, T.; Climent, V.; Armstrong, F. A. Electrochemical Mechanism of Reversible Hydrogen Cycling by Enzymes and Distinctions between the Major Classes of Hydrogenases. *Proc. Natl. Acad. Sci. U.S.A.* **2012**, *109*, 11516–11521.
- (2) Kleinhaus, J. T.; Wittkamp, F.; Yadav, S.; Siegmund, D.; Apfel, U. P. [FeFe]-Hydrogenases: maturation and reactivity of enzymatic systems and overview of biomimetic models. *Chem. Soc. Rev.* **2021**, *50*, 1668–1784.
- (3) Peters, J. W. X-ray Crystal Structure of the Fe-Only Hydrogenase (CpI) from *Clostridium pasteurianum* to 1.8 Å Resolution. *Science* **1998**, *282*, 1853–1858.
- (4) Nicolet, Y.; Piras, C.; Legrand, P.; Hatchikian, C. E.; Fontecilla-Camps, J. C. Desulfovibrio Desulfuricans Iron Hydrogenase: The Structure Shows Unusual Coordination to an Active Site Fe Binuclear Center. *Structure* **1999**, *7*, 13–23.
- (5) Silakov, A.; Wenk, B.; Reijerse, E.; Lubitz, W. 14N HYSOCORE Investigation of the H-Cluster of [FeFe] Hydrogenase: Evidence for a Nitrogen in the Dithiol Bridge. *Phys. Chem. Chem. Phys.* **2009**, *11*, 6592–6599.
- (6) Rodríguez-Maciá, P.; Pawlak, K.; Rüdiger, O.; Reijerse, E. J.; Lubitz, W.; Birrell, J. A. Intercluster Redox Coupling Influences Protonation at the H-Cluster in [FeFe] Hydrogenases. *J. Am. Chem. Soc.* **2017**, *139*, 15122–15134.
- (7) Kubas, A.; Orain, C.; De Sancho, D.; Saujet, L.; Sensi, M.; Gauquelin, C.; Meynial-Salles, I.; Soucaille, P.; Bottin, H.; Baffert, C.; Fourmond, V.; Best, R. B.; Blumberger, J.; Léger, C. Mechanism of O<sub>2</sub> Diffusion and Reduction in FeFe Hydrogenases. *Nat. Chem.* **2017**, *9*, 88–95.
- (8) Baffert, C.; Demuez, M.; Cournac, L.; Burlat, B.; Guigliarelli, B.; Bertrand, P.; Girbal, L.; Léger, C. Hydrogen-Activating Enzymes: Activity Does Not Correlate with Oxygen Sensitivity. *Angew. Chem., Int. Ed.* **2008**, *47*, 2052–2054.
- (9) Rodríguez-Maciá, P.; Galle, L. M.; Bjornsson, R.; Lorent, C.; Zebger, I.; Yoda, Y.; Cramer, S. P.; DeBeer, S.; Span, I.; Birrell, J. A. Caught in the H Inactive: Crystal Structure and Spectroscopy Reveal a Sulfur Bound to the Active Site of an O<sub>2</sub>-stable State of [FeFe] Hydrogenase. *Angew. Chem., Int. Ed.* **2020**, *59*, 16786–16794.
- (10) Rodríguez-Maciá, P.; Reijerse, E. J.; van Gestel, M.; DeBeer, S.; Lubitz, W.; Rüdiger, O.; Birrell, J. A. Sulfide Protects [FeFe] Hydrogenases From O<sub>2</sub>. *J. Am. Chem. Soc.* **2018**, *140*, 9346–9350.
- (11) Wait, A. F.; Brandmayr, C.; Stripp, S. T.; Cavazza, C.; Fontecilla-Camps, J. C.; Happe, T.; Armstrong, F. A. Formaldehyde-A Rapid and Reversible Inhibitor of Hydrogen Production by [FeFe]-Hydrogenases. *J. Am. Chem. Soc.* **2011**, *133*, 1282–1285.
- (12) Greco, C.; Bruschi, M.; Heimdal, J.; Fantucci, P.; De Gioia, L.; Ryde, U. Structural Insights into the Active-Ready Form of [FeFe]-Hydrogenase and Mechanistic Details of Its Inhibition by Carbon Monoxide. *Inorg. Chem.* **2007**, *46*, 7256–7258.
- (13) Stripp, S. T.; Goldet, G.; Brandmayr, C.; Sanganas, O.; Vincent, K. A.; Haumann, M.; Armstrong, F. A.; Happe, T. How Oxygen Attacks [FeFe] Hydrogenases from Photosynthetic Organisms. *Proc. Natl. Acad. Sci. U.S.A.* **2009**, *106*, 17331–17336.
- (14) Goldet, G.; Brandmayr, C.; Stripp, S. T.; Happe, T.; Cavazza, C.; Fontecilla-Camps, J. C.; Armstrong, F. A. Electrochemical Kinetic Investigations of the Reactions of [FeFe]-Hydrogenases with Carbon Monoxide and Oxygen: Comparing the Importance of Gas Tunnels and Active-Site Electronic/Redox Effects. *J. Am. Chem. Soc.* **2009**, *131*, 14979–14989.
- (15) Jones, A. K.; Sillery, E.; Albracht, S. P. J.; Armstrong, F. A. Direct Comparison of the Electrocatalytic Oxidation of Hydrogen by an Enzyme and a Platinum Catalyst. *Chem. Commun.* **2002**, *2*, 866–867.
- (16) Esmieu, C.; Raleiras, P.; Berggren, G. From protein engineering to artificial enzymes - biological and biomimetic approaches towards sustainable hydrogen production. *Sustainable Energy Fuels* **2018**, *2*, 724–750.
- (17) Rauchfuss, T. B. Diiron Azadithiolates as Models for the [FeFe]-Hydrogenase Active Site and Paradigm for the Role of the Second Coordination Sphere. *Acc. Chem. Res.* **2015**, *48*, 2107–2116.
- (18) Ding, S.; Ghosh, P.; Darensbourg, M. Y.; Hall, M. B. Interplay of Hemilability and Redox Activity in Models of Hydrogenase Active Sites. *Proc. Natl. Acad. Sci. U.S.A.* **2017**, *114*, E9775–E9782.
- (19) Mebs, S.; Kositzki, R.; Duan, J.; Kertess, L.; Senger, M.; Wittkamp, F.; Apfel, U. P.; Happe, T.; Stripp, S. T.; Winkler, M.; Haumann, M. Hydrogen and Oxygen Trapping at the H-Cluster of [FeFe]-Hydrogenase Revealed by Site-Selective Spectroscopy and QM/MM Calculations. *Biochim. Biophys. Acta, Bioenerg.* **2018**, *1859*, 28–41.
- (20) Bruska, M. K.; Stiebritz, M. T.; Reiher, M. Regioselectivity of H Cluster Oxidation. *J. Am. Chem. Soc.* **2011**, *133*, 20588–20603.
- (21) Swanson, K. D.; Ratzloff, M. W.; Mulder, D. W.; Artz, J. H.; Ghose, S.; Hoffman, A.; White, S.; Zadornyy, O. A.; Broderick, J. B.; Bothner, B.; King, P. W.; Peters, J. W. [FeFe]-Hydrogenase Oxygen Inactivation Is Initiated at the H Cluster 2Fe Subcluster. *J. Am. Chem. Soc.* **2015**, *137*, 1809–1816.
- (22) Esselborn, J.; Kertess, L.; Apfel, U. P.; Hofmann, E.; Happe, T. Loss of Specific Active-Site Iron Atoms in Oxygen-Exposed [FeFe]-Hydrogenase Determined by Detailed X-Ray Structure Analyses. *J. Am. Chem. Soc.* **2019**, *141*, 17721–17728.
- (23) Orain, C.; Saujet, L.; Gauquelin, C.; Soucaille, P.; Meynial-Salles, I.; Baffert, C.; Fourmond, V.; Bottin, H.; Léger, C. Electrochemical Measurements of the Kinetics of Inhibition of Two FeFe Hydrogenases by O<sub>2</sub> Demonstrate That the Reaction Is Partly Reversible. *J. Am. Chem. Soc.* **2015**, *137*, 12580–12587.
- (24) Lambertz, C.; Leidel, N.; Havelius, K. G. V.; Noth, J.; Chernev, P.; Winkler, M.; Happe, T.; Haumann, M. O<sub>2</sub> Reactions at the Six-iron Active Site (H-cluster) in [FeFe]-Hydrogenase. *J. Biol. Chem.* **2011**, *286*, 40614–40623.
- (25) Morra, S.; Arizzi, M.; Valetti, F.; Gilardi, G. Oxygen Stability in the New [FeFe]-Hydrogenase from *Clostridium Beijerinckii* SM10 (CbASH). *Biochemistry* **2016**, *55*, 5897–5900.
- (26) Corrigan, P.; Tirsch, J.; Silakov, A. Investigation of the Unusual Ability of the [FeFe] Hydrogenase from *Clostridium Beijerinckii* to Access an O<sub>2</sub>-Protected State. *J. Am. Chem. Soc.* **2020**, *142*, 12409–12419.
- (27) Roseboom, W.; De Lacey, A. L.; Fernandez, V. M.; Hatchikian, E. C.; Albracht, S. P. J. The Active Site of the [FeFe]-Hydrogenase from *Desulfovibrio Desulfuricans*. II. Redox Properties, Light Sensitivity and CO-Ligand Exchange as Observed by Infrared Spectroscopy. *J. Biol. Inorg. Chem.* **2006**, *11*, 102–118.
- (28) Glick, B. R.; Martin, W. G.; Martin, S. M. Purification and properties of the periplasmic hydrogenase from *Desulfovibrio desulfuricans*. *Can. J. Microbiol.* **1980**, *26*, 1214–1223.
- (29) Felbek, C.; Arrigoni, F.; de Sancho, D.; Jacq-Bailly, A.; Best, R. B.; Fourmond, V.; Bertini, L.; Léger, C. Mechanism of Hydrogen Sulfide-Dependent Inhibition of FeFe Hydrogenase. *ACS Catal.* **2021**, *11*, 15162–15176.

- (30) Winkler, M.; Duan, J.; Rutz, A.; Felbek, C.; Scholtysek, L.; Lampret, O.; Jaenecke, J.; Apfel, U.-P.; Gilardi, G.; Valetti, F.; Fourmond, V.; Hofmann, E.; Léger, C.; Happe, T. A Safety Cap Protects Hydrogenase from Oxygen Attack. *Nat. Commun.* **2021**, *12*, 756.
- (31) Zheng, L.; Baumann, U.; Reymond, J. L. An Efficient One-Step Site-Directed and Site-Saturation Mutagenesis Protocol. *Nucleic Acids Res.* **2004**, *32*, No. e115.
- (32) Akhtar, M. K.; Jones, P. R. Deletion of IscR Stimulates Recombinant Clostridial Fe-Fe Hydrogenase Activity and H<sub>2</sub>-Accumulation in *Escherichia Coli* BL21(DE3). *Appl. Microbiol. Biotechnol.* **2008**, *78*, 853–862.
- (33) Kuchenreuther, J. M.; Grady-Smith, C. S.; Bingham, A. S.; George, S. J.; Cramer, S. P.; Swartz, J. R. High-Yield Expression of Heterologous [FeFe] Hydrogenases in *Escherichia Coli*. *PLoS One* **2010**, *5*, No. e15491.
- (34) Bradford, M. M. A Rapid and Sensitive Method for the Quantitation of Microgram Quantities of Protein Utilizing the Principle of Protein-Dye Binding. *Anal. Biochem.* **1976**, *72*, 248–254.
- (35) Laemmli, U. K. Cleavage of Structural Proteins during the Assembly of the Head of Bacteriophage T4. *Nature* **1970**, *227*, 680–685.
- (36) Li, H.; Rauchfuss, T. B. Iron Carbonyl Sulfides, Formaldehyde, and Amines Condense to Give the Proposed Azadithiolate Cofactor of the Fe-Only Hydrogenases. *J. Am. Chem. Soc.* **2002**, *124*, 726–727.
- (37) Esselborn, J.; Lambertz, C.; Adamska-Venkatesh, A.; Simmons, T.; Berggren, G.; Noth, J.; Siebel, J.; Hemschemeier, A.; Artero, V.; Reijerse, E.; Fontecave, M.; Lubitz, W.; Happe, T. Spontaneous Activation of [FeFe]-Hydrogenases by an Inorganic [2Fe] Active Site Mimic. *Nat. Chem. Biol.* **2013**, *9*, 607–609.
- (38) Merrouch, M.; Hadj-Saïd, J.; Léger, C.; Dementin, S.; Fourmond, V. Reliable Estimation of the Kinetic Parameters of Redox Enzymes by Taking into Account Mass Transport towards Rotating Electrodes in Protein Film Voltammetry Experiments. *Electrochim. Acta* **2017**, *245*, 1059–1064.
- (39) Fourmond, V. QSoas: A Versatile Software for Data Analysis. *Anal. Chem.* **2016**, *88*, 5050–5052.
- (40) Abraham, M. J.; Murtola, T.; Schulz, R.; Páll, S.; Smith, J. C.; Hess, B.; Lindahl, E. Gromacs: High Performance Molecular Simulations through Multi-Level Parallelism from Laptops to Supercomputers. *SoftwareX* **2015**, *1–2*, 19–25.
- (41) Chang, C. H.; Kim, K. Density Functional Theory Calculation of Bonding and Charge Parameters for Molecular Dynamics Studies on [FeFe] Hydrogenases. *J. Chem. Theory Comput.* **2009**, *5*, 1137–1145.
- (42) McCullagh, M.; Voth, G. A. Unraveling the Role of the Protein Environment for [FeFe]-Hydrogenase: A New Application of Coarse-Graining. *J. Phys. Chem. B* **2013**, *117*, 4062–4071.
- (43) Bussi, G.; Donadio, D.; Parrinello, M. Canonical Sampling through Velocity Rescaling. *J. Chem. Phys.* **2007**, *126*, 014101.
- (44) Berendsen, H. J. C.; Postma, J. P. M.; van Gunsteren, W. F.; DiNola, A.; Haak, J. R. Molecular Dynamics with Coupling to an External Bath. *J. Chem. Phys.* **1984**, *81*, 3684–3690.
- (45) Páll, S.; Hess, B. A Flexible Algorithm for Calculating Pair Interactions on SIMD Architectures. *Comput. Phys. Commun.* **2013**, *184*, 2641–2650.
- (46) Darden, T.; York, D.; Pedersen, L. Particle mesh Ewald: An N-Log(N) method for Ewald sums in large systems. *J. Chem. Phys.* **1993**, *98*, 10089–10092.
- (47) Hess, B. P-LINCS: A Parallel Linear Constraint Solver for Molecular Simulation. *J. Chem. Theory Comput.* **2008**, *4*, 116–122.
- (48) Miyamoto, S.; Kollman, P. A. Settle: An Analytical Version of the SHAKE and RATTLE Algorithm for Rigid Water Models. *J. Comput. Chem.* **1992**, *13*, 952–962.
- (49) Heiby, J. C.; Goretzki, B.; Johnson, C. M.; Hellmich, U. A.; Neuweiler, H. Methionine in a Protein Hydrophobic Core Drives Tight Interactions Required for Assembly of Spider Silk. *Nat. Commun.* **2019**, *10*, 4378.
- (50) Aledo, J. C. Methionine in Proteins: The Cinderella of the Proteinogenic Amino Acids. *Protein Sci.* **2019**, *28*, 1785–1796.
- (51) Ravi, J.; Hills, A. E.; Cerasoli, E.; Rakowska, P. D.; Ryadnov, M. G. FTIR Markers of Methionine Oxidation for Early Detection of Oxidized Protein Therapeutics. *Eur. Biophys. J.* **2011**, *40*, 339–345.
- (52) Yashiro, H.; White, R. C.; Yurkovskaya, A. V.; Forbes, M. D. E. Methionine Radical Cation: Structural Studies as a Function of PH Using X- and Q-Band Time-Resolved Electron Paramagnetic Resonance Spectroscopy. *J. Phys. Chem. A* **2005**, *109*, 5855–5864.
- (53) Kudryavtseva, E. V.; Sidorova, M. V.; Ovchinnikov, M. V.; Bepalova, Z. D. Hydrogen Peroxide for Disulfide Bridge Formation in Methionine-Containing Peptides. *J. Pept. Sci.* **2000**, *6*, 208–216.
- (54) Gellman, S. H. On the Role of Methionine Residues in the Sequence-Independent Recognition of Nonpolar Protein Surfaces. *Biochemistry* **1991**, *30*, 6633–6636.
- (55) Katz, S.; Noth, J.; Horch, M.; Shafaat, H. S.; Happe, T.; Hildebrandt, P.; Zebger, I. Vibrational Spectroscopy Reveals the Initial Steps of Biological Hydrogen Evolution. *Chem. Sci.* **2016**, *7*, 6746–6752.
- (56) Sommer, C.; Adamska-Venkatesh, A.; Pawlak, K.; Birrell, J. A.; Rüdiger, O.; Reijerse, E. J.; Lubitz, W. Proton Coupled Electronic Rearrangement within the H-Cluster as an Essential Step in the Catalytic Cycle of [FeFe] Hydrogenases. *J. Am. Chem. Soc.* **2017**, *139*, 1440–1443.
- (57) Winkler, M.; Senger, M.; Duan, J.; Esselborn, J.; Wittkamp, F.; Hofmann, E.; Apfel, U. P.; Stripp, S. T.; Happe, T. Accumulating the Hydride State in the Catalytic Cycle of [FeFe]-Hydrogenases. *Nat. Commun.* **2017**, *8*, 16115.
- (58) Duan, J.; Senger, M.; Esselborn, J.; Engelbrecht, V.; Wittkamp, F.; Apfel, U. P.; Hofmann, E.; Stripp, S. T.; Happe, T.; Winkler, M. Crystallographic and Spectroscopic Assignment of the Proton Transfer Pathway in [FeFe]-Hydrogenases. *Nat. Commun.* **2018**, *9*, 1–11.
- (59) Boehr, D. D.; Schnell, J. R.; McElheny, D.; Bae, S. H.; Duggan, B. M.; Benkovic, S. J.; Dyson, H. J.; Wright, P. E. A Distal Mutation Perturbs Dynamic Amino Acid Networks in Dihydrofolate Reductase. *Biochemistry* **2013**, *52*, 4605–4619.
- (60) Tang, Q.-Y.; Kaneko, K. Long-Range Correlation in Protein Dynamics: Confirmation by Structural Data and Normal Mode Analysis. *PLoS Comput. Biol.* **2020**, *16*, No. e1007670.
- (61) Henzler-Wildman, K.; Kern, D. Dynamic Personalities of Proteins. *Nature* **2007**, *450*, 964–972.
- (62) Damnjanović, J.; Nakano, H.; Iwasaki, Y. Deletion of a dynamic surface loop improves stability and changes kinetic behavior of phosphatidylinositol-synthesizing Streptomyces phospholipase D. *Bio-technol. Bioeng.* **2014**, *111*, 674–682.
- (63) Yu, H.; Yan, Y.; Zhang, C.; Dalby, P. A. Two Strategies to Engineer Flexible Loops for Improved Enzyme Thermostability. *Sci. Rep.* **2017**, *7*, 1–15.
- (64) Gunasekaran, K.; Ma, B.; Nussinov, R. Triggering Loops and Enzyme Function: Identification of Loops That Trigger and Modulate Movements. *J. Mol. Biol.* **2003**, *332*, 143–159.
- (65) Herbert, C.; Schieberr, U.; Saxena, K.; Juraszek, J.; De Smet, F.; Alcouffe, C.; Bianciotto, M.; Saladino, G.; Sibrac, D.; Kudlinzki, D.; Sreeramulu, S.; Brown, A.; Rigon, P.; Herault, J. P.; Lassalle, G.; Blundell, T. L.; Rousseau, F.; Gils, A.; Schymkowitz, J.; Tompa, P.; Herbert, J. M.; Carmeliet, P.; Gervasio, F. L.; Schwalbe, H.; Bono, F. Molecular Mechanism of SSR128129E, an Extracellularly Acting, Small-Molecule, Allosteric Inhibitor of Fgf Receptor Signaling. *Cancer Cell* **2013**, *23*, 489–501.
- (66) Crean, R. M.; Biler, M.; van der Kamp, M. W.; Hengge, A. C.; Kamerlin, S. C. L. Loop Dynamics and Enzyme Catalysis in Protein Tyrosine Phosphatases. *J. Am. Chem. Soc.* **2021**, *143*, 3830–3845.
- (67) Malabanan, M. M.; Amyes, T. L.; Richard, J. P. A Role for Flexible Loops in Enzyme Catalysis. *Curr. Opin. Struct. Biol.* **2010**, *20*, 702–710.
- (68) Hammes-Schiffer, S.; Benkovic, S. J. Relating Protein Motion to Catalysis. *Annu. Rev. Biochem.* **2006**, *75*, 519.

(69) Moise, G.; Morales, Y.; Beaumont, V.; Caradonna, T.; Loria, J. P.; Johnson, S. J.; Hengge, A. C. A YopH PTP1B Chimera Shows the Importance of the WPD-Loop Sequence to the Activity, Structure, and Dynamics of Protein Tyrosine Phosphatases. *Biochemistry* **2018**, *57*, 5315–5326.

(70) Wang, L.; Goodey, N. M.; Benkovic, S. J.; Kohen, A. Coordinated Effects of Distal Mutations on Environmentally Coupled Tunneling in Dihydrofolate Reductase. *Proc. Natl. Acad. Sci. U.S.A.* **2006**, *103*, 15753–15758.

(71) Baxter, E. L.; Zuris, J. A.; Wang, C.; Vo, P. L. T.; Axelrod, H. L.; Cohen, A. E.; Paddock, M. L.; Nechushtai, R.; Onuchic, J. N.; Jennings, P. A. Allosteric Control in a Metalloprotein Dramatically Alters Function. *Proc. Natl. Acad. Sci. U.S.A.* **2013**, *110*, 948–953.

## Recommended by ACS

### Trapping of a Mononitrosyl Nonheme Intermediate of Nitric Oxide Reductase by Cryo-Photolysis of Caged Nitric Oxide

Hanae Takeda, Takehiko Tosha, *et al.*

JANUARY 05, 2023  
THE JOURNAL OF PHYSICAL CHEMISTRY B

READ 

### Irreversible Inactivation of Lactate Racemase by Sodium Borohydride Reveals Reactivity of the Nickel–Pincer Nucleotide Cofactor

Santhosh Gatreddi, Jian Hu, *et al.*

JANUARY 10, 2023  
ACS CATALYSIS

READ 

### Substrate-Gated Transformation of a Pre-Catalyst into an Iron-Hydride Intermediate $[(\text{NO})_2(\text{CO})\text{Fe}(\mu\text{-H})\text{Fe}(\text{CO})(\text{NO})_2)]^-$ for Catalytic Dehydrogenation of Dim...

Yu-Ting Tseng, Tsai-Te Lu, *et al.*

DECEMBER 29, 2022  
INORGANIC CHEMISTRY

READ 

### Serial Femtosecond Crystallography Reveals the Role of Water in the One- or Two-Electron Redox Chemistry of Compound I in the Catalytic Cycle of the B-Type Dye-Dec...

Marina Lučić, Jonathan A. R. Worrall, *et al.*

OCTOBER 18, 2022  
ACS CATALYSIS

READ 

Get More Suggestions >